ACS Sustainable Chemistry & Engineering

pubs.acs.org/journal/ascecg

Research Article

Energy Efficient Carbon Capture through Electrochemical pH Swing Regeneration of Amine Solution

Mu Lin, Clément Ehret, Hubertus V. M. Hamelers, Annemiek ter Heijne, and Philipp Kuntke*

Cite This: ACS Sustainable Chem. Eng. 2024, 12, 7309−7317

Read Online

ACCESS | Metrics & More | Article Recommendations | Supporting Information

ABSTRACT: Carbon capture is widely acknowledged as a promising strategy for achieving negative emissions. Electrochemical carbon capture technologies are considered a viable alternative to conventional temperature swing processes. Among these, employing the hydrogen oxidation and hydrogen evolution reactions as a redox couple, along with an ion exchange membrane, offers an effective means of establishing a pH swing for desorbing CO_2 and regenerating the alkaline solvent. However, the practical scalability of this approach is impeded by challenges such as high energy demands resulting from a high pH differential between anodic and cathodic environments and operation with solutions with a low conductivity, required to obtain an acceptable current yield. To address these limitations, this study introduces an innovative anion exchange membrane (AEM)-based electrochemical process for solvent regeneration. Our research demonstrates the advantageous utilization of amines as chemical buffers. Selecting an amine solution with a favorable pK_a (∼7 to 10) helps in maintaining bicarbonate as the predominant carbon species within the system, thereby ensuring a high current yield (>80%) across various operational conditions (current, load ratio, and solution concentration). Furthermore, our analysis indicates that the use of amine solutions effectively reduces the overpotential of the hydrogen evolution reaction due to a lower local pH. This results in a minimum energy requirement of 63 kJ/mol at a current density of 20 A/m^2 to regenerate the solution (MDEA) while maintaining high (>99%) product (CO_2) purity.

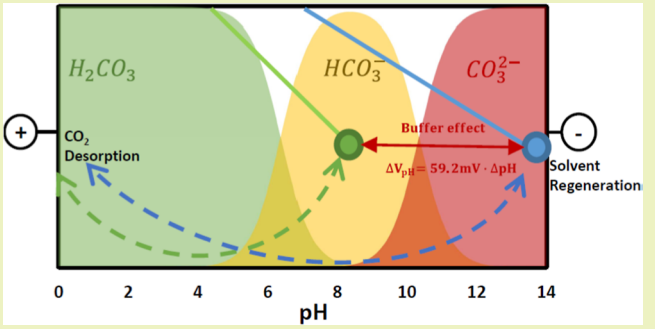

KEYWORDS: *carbon capture, electrochemical pH swing, amine solution regeneration, anion exchange membranes*

1. INTRODUCTION

Climate change refers to long-term shifts in the temperatures and weather patterns. Human activities have induced climate change through rapid industrial growth over the past 60 years. Particularly, carbon dioxide (CO_2) emissions contributed to such a shift.[1,2] In the last 60 years, the atmospheric concentration of CO_2 has increased by over 50% (from 280 to 420 ppm).[3,4] A general roadmap to reduce greenhouse gas emissions has been depicted by the Intergovernmental Panel on Climate Change (IPCC) and the International Energy Agency (IEA) to limit the global temperature rise to less than 2 °C by the year 2060.[5] This target could be reached by reducing the annual CO_2 emission by 75% compared to the current annual emissions (35 $GtCO_2$/year).[6] For this goal, efforts in technology development have been made in various directions: renewables, nuclear energy, and carbon capture, utilization, and storage (CCUS).[7]

CCUS refers to a technology portfolio that combines capturing and concentrating of CO_2 from diluted streams and processing (storage or conversion) of the enriched CO_2. These sources can either be atmospheric air (0.04%)[8] or more concentrated sources like flue gas (5−20%).[9] Currently, the state of art in postcombustion CO_2 capture technology is amine scrubbing with a thermal regeneration process. During this procedure, CO_2 is absorbed in by a counterflow contactor operating at temperatures ranging from 40 to 70 °C. Subsequently, the solvent (e.g., ethanolamine) is heated to 100−150 °C and then purified with steam to yield pure CO_2.[10] The high energy demands for such a regeneration process (typically 2.7−3 GJ/ton CO_2), which corresponds to approximately 20 to 30% of the power-generating capacity of a coal-powered plant, strongly hinder the proliferation of carbon capture facilities.[11] Furthermore, the technology suffers from the potential degradation of the amine solvents under high-temperature regeneration.[12] To overcome such challenges, there has been growing interest in developing electrochemical technologies that can reduce the energy consumption of carbon capture compared to that of this thermal amine carbon capture process. Electrochemical

Received: December 21, 2023
Revised: April 18, 2024
Accepted: April 19, 2024
Published: April 30, 2024

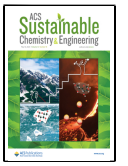

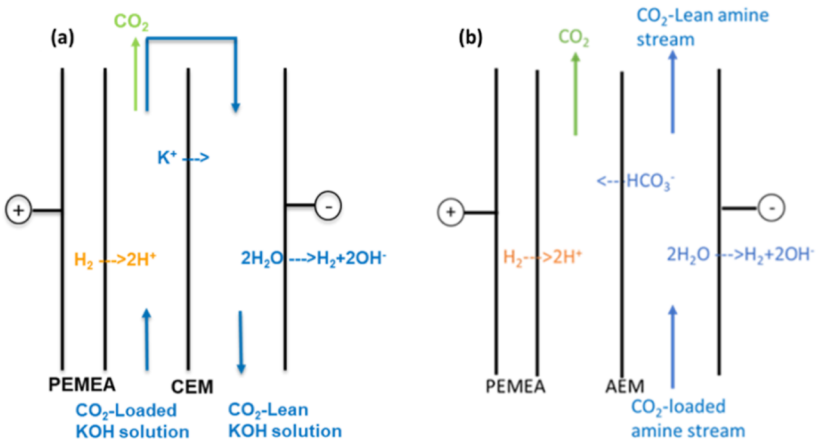

Figure 1. Spent alkaline solution regeneration by an electrochemical pH-swing process for carbon capture. (a) CO_2 rich alkaline solution regeneration in a CEM design (based on work of Shu et al., 2020[20]), (b) CO_2 rich amine solution regeneration in an AEM design (this study).

technologies allow for direct and efficient manipulation of CO_2—solution equilibria under room temperature. Furthermore, electrochemical technologies are more flexible in adapting to renewable energy due to their simpler integration with, for example, solar or wind-derived electricity.[13,14]

In general, carbon capture is a two-step process, namely, absorption and desorption. During the absorption step, CO_2 needs to be selectively separated from other gases usually with a bond formation. The subsequent desorption process releases CO_2 by breaking or replacing these bonds. With electrochemical technologies, such a principle has been applied in studies on quinone derivatives,[4,15,16] bipyridine,[17] and electrochemically mediated amine regeneration (EMAR) methods.[6,18] Another effective approach is to use protons as mediators in the absorption and desorption process. When absorption occurs, CO_2 (H_2CO_3) donates its proton(s) to a proton acceptor such as an alkaline solution (generalized $MOH_{(aq)}$), and bicarbonate (HCO_3^-) and/or carbonate (CO_3^{2-}) are formed ($H_2CO_3 + xMOH \leftrightarrow xM^+ + H_{(2-x)}CO_3^{x-}$, where x is either 1 or 2). By introducing protons into the system through an electrochemical oxidation reaction, HCO_3^-/CO_3^{2-} can be released as CO_2 from the solution $yH^+ + H_{(2-y)}CO_3^{(2-y)-} \leftrightarrow H_2CO_3$, (where y is either 1 or 2). The pH difference of the solution directly or indirectly induced by the electrode reactions in processes is known as an electrochemical pH swing.[19]

In general, the electrochemical pH swing solution regeneration process can benefit from prior knowledge obtained from (hydrogen) fuel cells (FCs) and water electrolyzers. A H_2-recycling electrochemical system (HRES) has first been used for nitrogen recovery from wastewater.[19] HRES is based on an anodic hydrogen oxidation reaction (HOR: $H_2 \rightarrow 2H^+ + 2e^-$) and a cathodic hydrogen evolution reaction (HER: $2H_2O + 2e^- \rightarrow 2OH^- + H_2$). Recently, a modified HRES has been demonstrated for the electrochemical pH swing carbon capture process using a cation exchange membrane (CEM).[20] This system for direct air capture was used to regenerate spent NaOH solution, as shown in Figure 1a. The rich solution was regenerated by H^+ ions released from the HOR in the acidifying compartment, leading to the release of CO_2. Subsequently, the solution's alkalinity was restored through OH^- ions from the HER in the cathode compartment, resulting in the production of a lean (alkaline) solution. The minimum theoretical voltage needed to establish an electrochemical pH swing is determined by the pH difference between the anode and cathode compartment considering a potential drop of 59.2 mV per pH unit (eq 1).[21]

$$V_{pH} = 2.303 \cdot \frac{R \cdot T}{F} \cdot \Delta pH = 0.0592 \cdot \Delta pH \quad (1)$$

where R is the ideal gas constant [8.314 J/(K mol)], T is the room temperature in Kelvin (297.15 K), F is the Faraday constant (96,485 C/mol), and 2.303 is the conversion factor from ln to $\log_{10}$. Our investigation has revealed that operating at a low load ratio results in a low current yield, as the introduced protons predominantly react with carbonate to form bicarbonate. Only at a specific load ratio threshold does the production of CO_2 commence. Consequently, it becomes energetically inefficient to regenerate only a portion of CO_2 from the solution. High recovery rate, however, requires a substantial pH shift: during extensive NaOH regeneration, the cathodic compartment experiences a highly alkaline pH (12−14). The introduction of the AEM system (Figure 1b) could resolve such a dilemma. In an AEM system, the current will transport the bicarbonate/carbonate to the acidifying compartment even at a low load ratio. The remaining of the unregenerated bicarbonate could possibly serve as the buffer to lower the local pH. Such an AEM system has recently been studied and demonstrated efficient by Muroyama et al.[22,23] However, OH^- formed in the HER will complete with bicarbonate and carbonate ions for transport through the AEM, resulting in a reduction in the current yield. This is also reported by Muroyama et al.[23] In theory, the utilization of amine-based solutions has the potential to address this issue. The presence of amines, typically characterized by pK_a values between 7 and 9, leads to a limitation in OH^- concentration due to the amine buffering effect. The reduction in OH^- concentration not only enhances the current yield but also impacts the HER redox potential, thereby lowering the overall applied cell voltage. This buffering effect has been extensively discussed within the fuel cell community over the past decade.[24−29] In essence, the incorporation of a buffering agent offers advantages by lowering the local pH at the electrode and reducing the concentration overpotential.

In this context, we studied an AEM-based electrochemical regeneration system with amines as the solution. We show the proof of concept and insights into the reduction in energy

https://doi.org/10.1021/acssuschemeng.3c08430
ACS Sustainable Chem. Eng. 2024, 12, 7309−7317

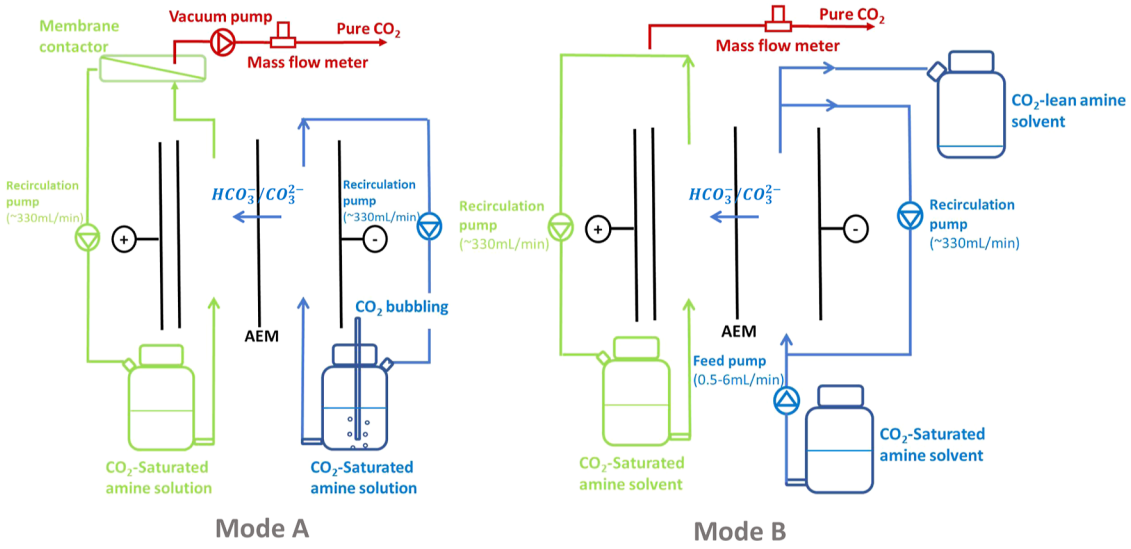

Figure 2. Illustrations of two different operation modes. Mode A: idealized process with constant saturated solution stream with vacuum pump (0.1 bar) and membrane contactor; mode B: continuous process with different load ratio scenarios without a vacuum pump and membrane contactor. In both modes, CO_2 is transported as the form of carbonate/bicarbonate from the cathodic compartment (blue) to the acidifying compartment (green) and released as CO_2 gas stream (red).

input by applying an amine buffered system for the HRES pH swing solution generation process.

2. EXPERIMENTAL SECTION

2.1. Experimental Methodology. *2.1.1. Experimental Setup.* As shown in Figure 1b, the regeneration setup was composed of three compartments: the cathodic compartment, the acidifying compartment, and the anodic compartment, which are separated by an anion exchange membrane (AEM) and a proton exchange membrane electrode assembly (PEMEA). A PEMEA consisting of a 15 × 15 cm^2 Nafion 117 cation exchange membrane integrated with a 10 × 10 cm^2 platinum-coated gas diffusion layer (0.5 mg_{Pt}/cm^2) (FuelCellEtc, TX) was applied as an anode, which separated the H_2 stream from the acidifying compartment. The AEM separating the acidifying compartment from the cathodic compartment was separated by a Fujifilm type-I membrane (Tilburg, The Netherlands). A platinum-coated mesh electrode (2.5 mg/cm^2, 10 × 10 cm^2, Magneto Special Anodes BV, The Netherlands) was applied as the cathode. An identically sized Ru/Ir-coated (0.5 mg/cm^2) titanium mesh electrode was applied as the current collector for the anode (Magneto Special Anodes BV, The Netherlands).

At the anode, H_2 entered the gas diffusion layer of PEMEA, and HOR introduced protons in the acidifying compartment. At the cathode, the HER regenerated the alkalinity of the solution. In theory, for every mole of H_2 consumed in the anode, 1 mol of H_2 is generated in the cathode, resulting in a net zero production of H_2 in theory. For practical reasons, H_2 was fed to the anodic compartment from a gas cylinder (99.99%, AIR PRODUCTS, The Netherlands) externally, and the H_2 generated from the cathode was not recycled.

Protons produced at the anode are transported through the PEM to the acidifying compartment, where they combine with bicarbonate/carbonate transported through the AEM to form CO_2. In the outflow of the acidifying compartment, a membrane contactor (Liqui-Cel EXF model 2.5 in. × 8 in., 3M, Germany) was applied for the gas−liquid (CO_2-solution) separation. The CO_2 gas produced was first passed through a Nafion tubing (TUB-0003, CO2Meter.com, FL, USA) to remove the water vapor from the samples. Finally, gas production was measured using a mass flow meter (EL-FLOW Prestige FG-111B, Bronkhorst, The Netherlands), which measures the gas mass flow and displays results in normalized flow rate (mLn/min). Gas purity was assessed using an infrared CO_2 sensor (SmartGAS Flow EVO, Germany) and validated by a micro gas chromatograph (Varian CP-4900, Agilent, CA, USA). Two peristaltic pumps (Masterflex L/S, Metrohm, The Netherlands) were used for solution recirculation in the experimental setup: one for the acidifying compartment and one for the cathodic compartment. Both pumps were set to a flow rate of 330 mL/min (~10 cm/s).

The anode (PEMEA) potential and cathode potential were measured versus two Ag/AgCl reference electrodes (+0.23 V vs SHE) (ProSense B.V., The Netherlands). The pH of the solution was measured using a pH sensor (digiLine, JUMO GmbH and Co, Fulda, Germany). Galvanostatic control was carried out by using a potentiostat (Vertex.10A, IVIUM, The Netherlands). Two conductivity sensors (JUMO digiLine Ci HT10, Germany) were used to measure the conductivity. All sensors were placed at the exit of the electrochemical cell in the acidifying and cathodic compartment. The amine concentration in the solution was measured by ion chromatography (761 Compact IC, Metrohm, Switzerland).

2.1.2. Experimental Procedure. Three different amines, ethanolamine (MEA, ≥99% purity), diethanolamine (DEA, ≥98% purity), and methyl diethanolamine (MDEA, ≥99% purity), were investigated in this study. These three amines are widely applied in the postcombustion carbon capture practice and also represent the different amine classes: primary, secondary, and tertiary amines, respectively. All chemicals used in this research were purchased from Sigma-Aldrich and used without further purification.

2.1.3. Current Yield and Ohmic Resistance. Figure 2 depicts the two different operation modes designed to understand the system performance. Experiments (mode A, Figure 2) were carried out to understand the current yield and ohmic resistance across different concentrations of amine solutions (0.5, 1, 1.5, and 2 M) under different current densities (0, 20, 40, 60, 80, and 100 A/m^2). The current yield (r_i) is described as the ratio between the equilibrium current corresponding to the amount of CO_2 production versus the actual current applied as eq 2.

$$r_i = \frac{\frac{q_{CO_2}}{V_m}}{\frac{j_c \cdot A}{F}} \tag{2}$$

where j_c is the applied current density (A/m^2), q_{CO_2} is the CO_2 production rate (L/s), V_m is the normalized molar gas volume (22.4 L/mol), and A is the active AEM membrane area (0.01 m^2). The r_i is a measurement of overall current efficiency.

Each experiment at a given current density took ~6 h to ensure steady state was established. Blank experiments with the same

https://doi.org/10.1021/acssuschemeng.3c08430
ACS Sustainable Chem. Eng. 2024, 12, 7309−7317

concentration (current density 0 A/m^2) were carried out and the CO_2 production from the blank experiments was subtracted from the corresponding experimental groups. This production of CO_2 was due to the diffusion transport of CO_2 (H_2CO_3) through the AEM from the concentration differences: in the cathodic compartment, the solution was in equilibrium with pure CO_2, whereas in the acidifying compartment, the solution was in equilibrium with ambient air.

To provide a realistic energy consumption assessment, we examined the system with a set of experiments (mode B, Figure 2) that were performed by fixing the current density and adjusting the CO_2 rich amine solution flow rate. In this case, we actively controlled the expected lean loading of solution in the effluent, i.e., create different scenarios for the extent of solution regeneration. Arguably these experiments mimicked operational scenarios which recovered CO_2 from a 100% purity CO_2 input. However, it was noteworthy that in a continuous process, the energy consumption was only subjective to the carbon loading of the effluent and not of the influent. In operation mode B, we also removed the vacuum pump and the membrane contactor. CO_2 was stripped under the atmospheric pressure.

Here, we introduced the cation load ratio (L_c) to better describe operation mode B. L_c was a factor defined by the ratio of current density and the theoretical equilibrium current density required to remove all the carbonate and bicarbonate ions

$$L_c = \frac{j_C \cdot A}{C_{cation,0} \cdot Q \cdot F} \tag{3}$$

where j_C is the applied current density (A/m^2), A is the active AEM membrane area (0.01 m^2), the $C_{cation,0}$ is the molar concentration of cation (deprotonated MDEA or potassium K^+ in this study) in the influent solution (mol/m^3), Q is the flow rate of the influent solution (m^3/s), and F is the Faraday constant (96,485 C/mol). When $L_c = 1$, it implies the supplied current can transport all carbonate or bicarbonate ions introduced in the system. When $L_c < 1$, it implies the supplied current was not sufficient to transport all the carbonate or bicarbonate ions introduced in the system. Compared with the experiments of mode A, CO_2 was not continuously supplied to the amine solution. In both modes, energy consumption (E.C.) is defined and calculated according to eq 4.

$$\text{E. C.} = \frac{j_c \cdot A \cdot U}{\frac{q_{CO_2}}{V_m}} \tag{4}$$

where j_C is the applied current density (A/m^2), A is the active AEM membrane area (0.01 m^2), U represents the measured overall voltage (V) without iR compensation, q_{CO_2} is the CO_2 production rate (L/s), and V_m is the normalized molar gas volume (22.4 L/mol).

In general, operation Mode A provides us an ideal operational condition for the electrochemical cell performance where the concentration of the studied rich solution remains the same in the influent, the cathodic compartment, and in the effluent. Operation mode B represents scenarios where the carbonic concentrations in the amine solutions were identical in the cathodic compartment and in the effluent, while different from those in the influent, and the concentration difference depends on the load ratio. Therefore, mode B represents a more realistic application scenario.

2.2. Polarization Curve Modeling for Cathode. To understand the effect of an amine buffer on overpotential for the HER, five different CO_2-saturated solutions (1 M MDEA, DEA, MEA, $KHCO_3$, and 0.5 M K_2CO_3) and KOH solutions were tested in mode A. In each experiment, the aforementioned identical solutions were recirculated in both the acidifying compartment and the cathodic compartment. To ensure equal (across the AEM) and constant concentrations of bicarbonate and carbonate species, CO_2 was continuously supplied to the cathodic tank during the whole experiment for the groups of MDEA, DEA, MEA, and $KHCO_3$ to ensure the saturation state of the solutions. For K_2CO_3, the solution recirculated in the cathodic compartment was replenished every 2 h during the experiment.

The current density was stepwise increased from 0 to 75 A/m^2, and the potential difference between the reference electrode and the cathode was recorded. Each step was maintained for 1 h to reach equilibrium, and the potential was measured every 5 s. The average of the potential measurements of the last 30 min was used to calculate the cathode potential.

A simple model was applied to describe the electrode potential measured in this study to understand the effect of the amine buffer. In this model, the electrode potential measured consists of the equilibrium potential (E_{eq}), the activation overpotential (η_{act}), the ohmic overpotential (η_{ohm}), and the contribution of mass transfer limitations. Due to the low current density applied ($j \leq 75$ A/m^2), mild concentration (1 M), and higher linear flow velocities (~10 cm/s) in this study, mass transfer limitations were excluded from the model. Therefore, the cathode potential ($V_{cathode}$) was described according to eq 5.[30]

$$V_{cathode} = E_{eq} + \eta_{act} + \eta_{ohm} \tag{5}$$

The equilibrium potential is defined by Nernst Equation (eq 6)

$$E_{eq} = E^0 + \frac{R \cdot T}{z \cdot F} \cdot \ln\left(\frac{[\text{Red}]}{[\text{Ox}]}\right) \tag{6}$$

where z is the number of electrons transferred in the redox reaction. After the species of the redox reaction (HER) is substituted in the Nernst equation (eq 6), the equilibrium can be rewritten as eq 7

$$E_{eq} = 0.0592V \cdot \text{pH}_{cathode} \tag{7}$$

The activation energy is represented with the Tafel equation (eq 8)[31]

$$\eta_{act} = -\frac{R \cdot T}{\alpha \cdot F} \cdot \ln|j| + \frac{R \cdot T}{\alpha \cdot F} \cdot \ln|j_0| = a \cdot \ln|j| + b \tag{8}$$

where α is the charge transfer coefficient, j is the current density (A/m^2), j_0 is the exchange current density (A/m^2), a represents the Tafel slope. With the assumption of a fixed electric resistance (R_{Ohmic}) within the current density range in this study, the ohmic overpotential (η_{Ohm}) is represented by a linear equation in eq 9

$$\eta_{Ohm} = j_c \cdot R_{Ohmic} \cdot A \tag{9}$$

where j_C is the current density, and A is the active cross-section area m^2.

With the voltage−current ($U-I$) response measurement, the model was completed with the following steps. First, we used the data of the response from the higher current density (20−75 A/m^2) to plot a linear regression line, the slope of which was determined as the ohmic resistance (R_{Ohmic}). Next, we calibrated the potential responses by deducting the ohmic potential ($U - j_C \cdot R_{Ohmic} \cdot A$), and the results represent the sum of activation overpotential and equilibrium potential. We plotted a linear regression line with the corrected potential toward the current density. The slope and the y-intercept were used to calculate the charge transfer coefficient (α) and exchange current density (j_0). Finally, we simulated the polarization curve with the values mentioned above and calculated the correlation coefficient (R^2) between the model and the experimental data. In addition to the model, which incorporates the measured conductivity (σ), and assuming a homogeneous layer, the calculated ohmic resistance ($R_{Ohmic,c}$) attributed by the electrolyte can be calculated using eq 10, where the compartment thickness is taken as the spacer thickness (t = 0.43 mm)

$$R_{Ohmic,c} = \frac{A}{\sigma \times t} \tag{10}$$

3. RESULTS AND DISCUSSIONS

3.1. Amine Concentrations and Current Density Impact AEM System Performance. To get a better understanding of the overall performance for the AEM system with different loaded solutions, we analyzed two different

https://doi.org/10.1021/acssuschemeng.3c08430
ACS Sustainable Chem. Eng. 2024, 12, 7309−7317

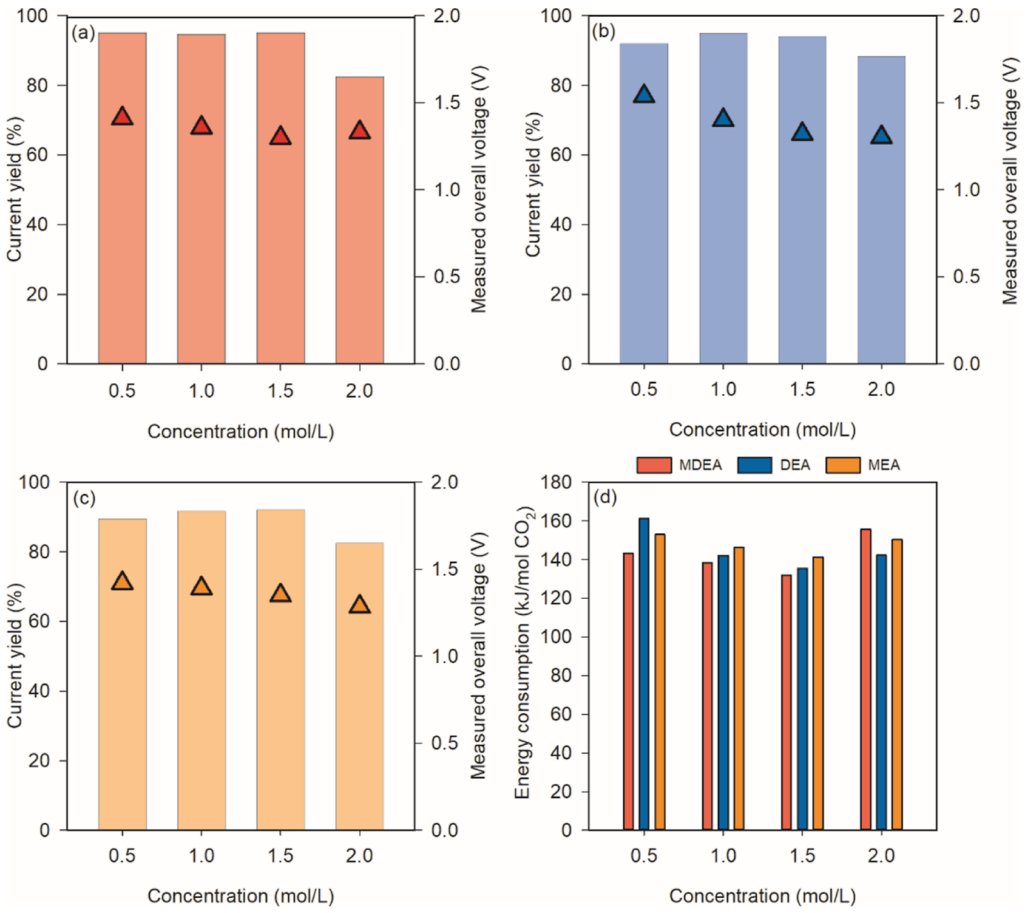

Figure 3. Current yield (r_i) and measured cell voltage with increased concentration of saturated (a) MDEA, (b) DEA, and (c) MEA solution at a current density of 100 A/m^2 under operation Mode A (bar chart: Current yield; symbols ▲: Measured overall voltage); (d) overview of the energy consumption for all cases.

operational modes (A and B) with different loaded solutions. In both sets of experiments, a CO_2 purity higher than 99% was reached. Amines were not degraded during the experiments (no detectable concentration losses when analyzed by ion chromatography), with the longest operational windows of 7 days.

The overall performance in operation mode A with different amine concentrations is shown in Figure 3. By increasing the amine concentration from 0.5 to 2 M, overall, the measured cell voltage decreases for all cases. This could be explained by the gains from the increasing conductivity (related to the decreasing R_{Ohmic}). The current yield (r_i) remained >95% for all cases among the groups of 0.5, 1, and 1.5 M. A decrease of r_i was observed when the concentration increased to 2 M. We suspected that at this high concentration, the AEM lost selectivity and did not act as an effective selective barrier and protonated amine transport occurred to a higher extent compared to the group with lower concentrations.[32] In terms of energy consumption, a decrease was expected when we increased the concentration until a certain degree due to the increase in conductivity without loss in r_i. However, at the highest amine concentration, there was an increase in energy consumption, most likely due to the loss of r_i.

Among the three amines considered, MDEA demonstrated a slight advantage in terms of both the current yield and energy consumption. This advantage can be attributed to MDEA's tertiary amine characteristics, resulting in a higher bicarbonate content in the saturated solution. In contrast, primary and secondary amines such as MEA and DEA tend to form carbamates, which contribute to a reduction in current yield. It is noteworthy that carbamate ions ($R_1NH-CO_2^-$, $R_1R_2N-CO_2^-$ in our case) can permeate through the AEM to produce CO_2, upon binding with protons. The regenerated amine (R_1NH_2, R_1R_2NH) can undergo further protonation, as illustrated in eqs 11−14. This could lead to a loss of the current yield. However, the overall differences between the amines were not significant, suggesting a high compatibility between different classes of amines and the proposed AEM process.

$$R_1NH - CO_2^- + H^+ \rightarrow R_1NH_2 + CO_2 \quad (11)$$

$$R_1NH_2 + H^+ \rightarrow R_1NH_3^+ \quad (12)$$

$$R_1R_2N - CO_2^- + H^+ \rightarrow R_1R_2NH + CO_2 \quad (13)$$

$$R_1R_2NH + H^+ \rightarrow R_1R_2NH_2^+ \quad (14)$$

Figure 4 shows the overall performance of operation mode A at various current densities (0−100 A/m^2). With all three amines at a concentration of 0.5 M, the current yield remained >90% for all cases. Particularly, we reached a current yield of 98.6% at 20 A/m^2 for MDEA with an energy consumption as low as 63 kJ/mol. For all amines, with an increasing current density, the energy consumption for all groups increased due to the increase in applied voltage (Figure S1). The increase in the applied voltage will be further discussed in the next section.

https://doi.org/10.1021/acssuschemeng.3c08430
ACS Sustainable Chem. Eng. 2024, 12, 7309−7317

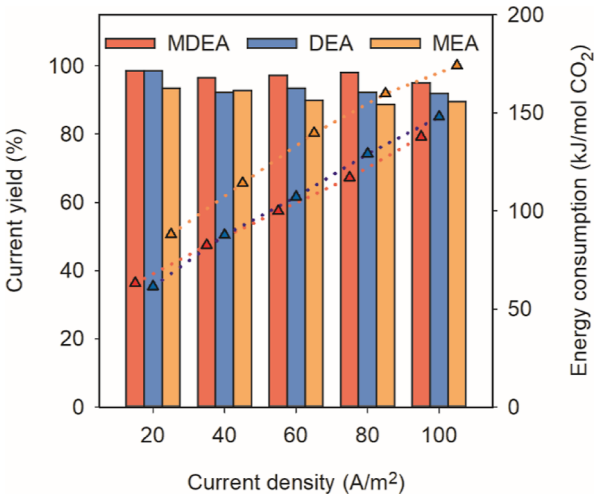

Figure 4. Current yield (r_i) and energy consumption under different current densities with three different amines (0.5 M) under operation mode A (symbols -▲-: Energy consumption; bar chart: Current yield).

These findings highlight the efficiency of operation mode A in maintaining high current yields across various current densities and different amines.

3.2. MDEA Stabilizes Current Yield and Energy Consumption in a Continuous Operation. For the study of mode B, we compared performances among 1 M saturated MDEA, 1 M $KHCO_3$, and 0.5 M K_2CO_3 at a current density of 100 A/m^2. As shown in Figure 5, a lower current yield (~10%) was observed compared to that of mode A operation. Inadequate removal of CO_2 without the vacuum and membrane contactor may explain this minor decrease: without the vacuum and the membrane contactor, the formed H_2CO_3 did not transform to CO_2 fast enough, and partly diffused back to the cathodic compartment due to the concentration difference of H_2CO_3 between cathodic compartment and acidifying compartment.

We also observed a minor pH increase in the acidifying compartment after removing the vacuum and the membrane contactor (from 7.8 to 8.0) which indicates a higher concentration of carbon species in the steady state. MDEA had a stable performance in terms of current yield (r_i > 0.8 for all scenarios) across different load ratios while current yields for K_2CO_3 and $KHCO_3$ were largely affected by the increasing load ratio, 0.91−0.64 and 0.34−0.14, respectively. The difference was due to the buffer effect, MDEA has a pK_a of 8.5 while bicarbonate/carbonate pK_{a2} is 10.3. With MDEA, the dominant carbon species in the cathodic compartment will remain HCO_3^- [protonated MDEA (eq 15), will take up the OH^- instead of HCO_3^- (eq 16)]. Without MDEA present, the bicarbonate will transform to carbonate when it reacts with OH^-. Thus, the concentration of carbonate ions (CO_3^{2-}) will increase with an increasing load ratio. This could also be well verified with the pH increase from Figure 5c. The pH increased from 8.1 to 9.4 for the MDEA group, and 9.0 to 10.4 for the carbonate group. Assuming the steady state is also the chemical equilibrium state, this translates to an increase of carbonate species in the carbon system from 4.4 to 53.5% for the group of $KHCO_3$, and only 0.6−10.3% for the MDEA system. As explained earlier, the transfer of 1 mol of carbonate to the acidifying compartment requires twice the current as the transfer of 1 mol of bicarbonate, for the same carbon removal.

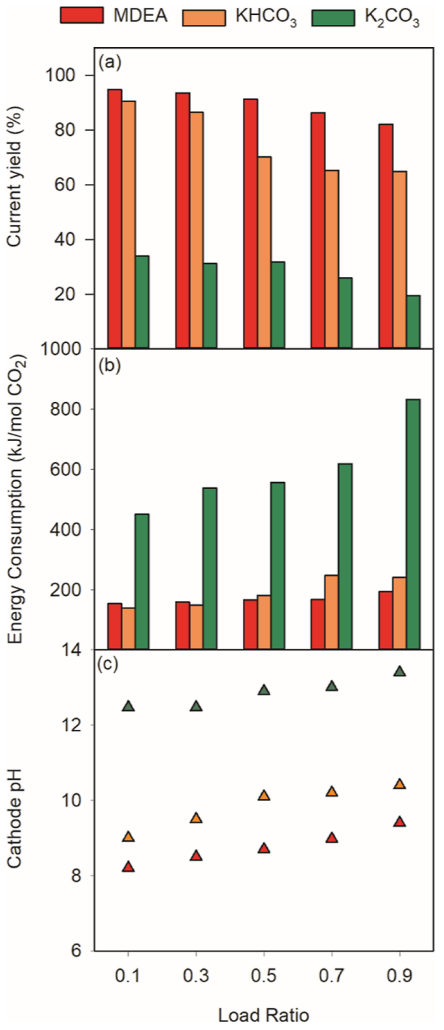

Figure 5. Overall performance in operation mode B with different solutions at different load ratios: (a) Current yield; (b)Energy Consumption; (c) pH of the cathode compartment at steady state.

This will significantly lower the current yield, which aligns very well with the results shown in Figure 5a.

$$A - H^+ + OH^- \rightarrow A + H_2O \quad (15)$$

$$HCO_3^- + OH^- \rightarrow CO_3^{2-} + H_2O \quad (16)$$

With the K_2CO_3 group, OH^- concentration increases with increasing load ratios in the cathodic compartment, the competition for transport between OH^- and carbonate species HCO_3^-, CO_3^{2-} intensifies, and results in a decrease of current yield. Besides the attribution from the current yield decrease with the increasing load ratio, the increase of the overall voltage in general is another aspect that determines energy consumption (Figure S2). We suspect that the increase in cell voltage is due to the increase in membrane potential as a result of the HCO_3^- concentration differences buildup across the AEM.

In Figure 5b, we obtained a better sense of how the overall energy consumption varied with different load ratios (L_c). At a current density of 100 A/m^2, the energy consumption for the MDEA group was relatively stable (154−194 kJ/mol) compared to the group of $KHCO_3$ (140−262 kJ/mol), the group of K_2CO_3 behaves the worst among all groups, and

https://doi.org/10.1021/acssuschemeng.3c08430
ACS Sustainable Chem. Eng. 2024, 12, 7309−7317

energy consumption was both high and unstable across different load ratios (451−1148 kJ/mol).

A regeneration step is employed to reclaim a portion of dissolved CO_2, with the regenerated solution being returned to initiate a new absorption cycle. If the recovered CO_2 fraction is insufficient (resulting in a higher rich loading in the effluent from the regeneration process), it adversely affects the kinetics of the subsequent absorption process. Therefore, achieving a higher CO_2 recovery rate is desirable for the overall process. In terms of energy consumption, it is noteworthy that MDEA demonstrated greater stability across a wide range of load ratios compared to that of KOH as a solution.

In practical applications, achieving full saturation of the solution with CO_2, known as a rich loading of 100%, is rare. Instead, it is customary to anticipate a rich loading ranging from 30 to 70%, as reported in several studies.[33−36] In general, any regeneration process is expected to produce an effluent with a lower carbon loading. As the energy consumption of our system was dependent on the carbon loading of the effluent and not on the influent, its performance can be directly correlated with different load ratios. This highlights the benefits of MDEA compared to KOH as a solution, as MDEA demonstrates stable performance characteristics over a wider range of regeneration scenarios (i.e., load ratios).

3.3. Buffer Effect Lowers the Cathodic Overpotential.

The polarization curve fitting is shown in Figure 6, we noticed

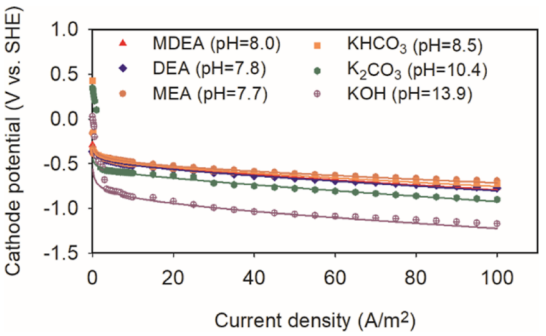

Figure 6. Cathode polarization curves with different solutions operating under mode A (symbols ●: experimental data; lines: model results).

a displacement of the cathode potential toward more positive values relative to the pH: the groups of all three saturated amine (pH = 7.7−8) and the $KHCO_3$ (pH = 8) have higher potentials than the K_2CO_3 group (pH = 10.4), and the KOH group (pH = 13.9) has the lowest potential among all groups. The strong correlation coefficient (R^2) provided in Table 1 further confirms the robustness of this fit.

The displacement of the cathodic potential among all groups can be attributed by the difference in the sum of the equilibrium potential (E_{eq}) and the constant part of the activation potential in the Tafel model (b), ($E_{eq} - b$) (Table 1). One way of looking at it is that buffer (either bicarbonate or protonated amine) efficiently removes the OH^- produced by the HER process which keeps the local pH on the cathode sufficiently low. The other way to consider such an effect is that protonated amine and bicarbonate species can directly donate their protons to produce H_2 due to the lower binding energy with the protons compared to water molecules.[37] The buffer effect strongly depends on the proton-binding energy of the proton-donating species, which is denoted as their pK_a (the acid dissociation constant).[21]

Despite bicarbonate and protonated amine having a similar pK_a and acting as buffers for the system, the performance of the process can differ as shown in the results of the continuous experiments (mode B). At a lower load ratio of regeneration, fully saturated KOH ($KHCO_3$ group) even has a slightly better performance in terms of the energy consumption due to a lower voltage required, and this could be due to the conductivity improvement (Table 1). It is noteworthy that during the increase of the load ratio, the product concentration from the buffer reaction increases. While for the amine group, the major product is deprotonated amine, for the $KHCO_3$ group, the major product is carbonate. Carbonate and hydroxyl will decrease the current yield while deprotonated amine will not. That could explain a more stable current yield and energy consumption across a wider load ratio for the MDEA group. But both (KOH and amine) suffer from a current yield loss due to the increase of the hydroxyl concentration at a higher load ratio where the buffer concentration is low.

The key parameters and measured solution parameters are summarized in Table 1. If we consider the electrolyte as a homogeneous system, with no ion concentration differences across the compartment, the Ohmic resistance calculated from the measured conductivity ($R_{Ohmic,c}$) only attributed to less than 12% of the total resistance shown in the model ($R_{Ohmic,m}$). The greater part of the resistance is suspected to be attributed by other factors such as bubble formation[22,38] and conductivity decrease due to bubble formation. Bubbles, being non-conductive, can create voids within an electrolyte, increasing the local current density, also hindering the contact between the electrolyte and the electrode. A promising direction worth investing is to optimize the degassing process for both hydrogen and carbon dioxide.[22,23,38,39] It is noteworthy that

Table 1. Model Results for the Key Parameters and Measured Solution Parameters[a]

parameter	DEA	MEA	MDEA	K_2CO_3	$KHCO_3$	KOH
Tafel slope a (mV/dec)[b]	−82.1	−92.1	−80.7	−70.6	−78.7	−146.5
transfer coefficient α[b]	0.72	0.64	0.73	0.84	0.75	0.40
$E_{eq} - b$ (V)[b]	−0.58	−0.58	−0.56	−0.66	−0.56	−1.00
model $R_{Ohmic,m}$ (mΩ)[b]	230.0	155.5	230.0	265.2	219.2	222.7
coefficient of determination (R^2)[b]	99.6%	98.7%	99.6%	99.0%	99.4%	97.5%
measured conductivity (mS/cm)	23.7	24.2	23.8	97.4	76.4	188.8
calculated $R_{Ohmic,c}$ (mΩ)	18.1	17.8	18.1	4.4	5.6	2.3
conductivity contribution	7.9%	11.4%	7.9%	1.7%	2.6%	1.0%

[a]The experiments were conducted under standard conditions (T = 298 K, P = 1 atm) using 1 M concentrations of KOH, $KHCO_3$, saturated amine, and 0.5 M concentration of K_2CO_3. [b]Indicates model results.

https://doi.org/10.1021/acssuschemeng.3c08430
ACS Sustainable Chem. Eng. 2024, 12, 7309−7317

minimizing the resistance holds significance in reducing energy consumption at higher current densities, further studies should clarify internal resistance dynamics by employing electrical resistance measurements such as electrical impedance spectroscopy.[40] Studies on PEM fuel cell and AEM fuel cell can serve as strong references refs 41 and 42. In summary, the model underscores the correlation between the enhancements facilitated by utilizing amines as the solution and the reduction in the HER potential attributed to the buffer effect. Additionally, the model reveals a relatively high calculated resistance (R_{Ohmic}), warranting further investigation. Compared to the state-of-the-art thermal regeneration process for amine scrubbing, the use of amines and the adjustable pH swing in the electrochemical process offer the potential for increased energy efficiency. However, a critical hurdle to overcome lies in comprehending and mitigating the ohmic resistance, which is imperative for realizing the full energy-saving advantages of the electrochemical approach.

4. CONCLUSIONS

The proposed AEM-based electrochemical system demonstrated a very low energy demand for regenerating the loaded-alkaline amine sorbent stream used for carbon capture. The system produced CO_2 with high purity (>99%). We successfully demonstrated an energy consumption as low as 63 kJ/mol CO_2 at a current density (20 A/m^2) and a high adaptability toward various amine classes. In our continuous study, MDEA showed a stable performance and superior energy efficiency compared to KOH in recovering CO_2 under various load ratios. Our polarization curve measurements demonstrated that both amine and bicarbonate acted as effective buffers, elevating cathodic potential and consequently reducing energy consumption. Notably, amines, as employed in our system, retain the advantage over KOH solution due to the difference of their buffering properties, while protonated amines have no detrimental impact on current yield, carbonate does have detrimental impacts. We also highlighted the electrochemical cell's resistance as an important barrier to investigate and improve for further reduction in energy consumption.

■ ASSOCIATED CONTENT

Supporting Information

The Supporting Information is available free of charge at https://pubs.acs.org/doi/10.1021/acssuschemeng.3c08430.

Cell voltage and energy consumption at different current densities with three different amines (0.5 M) under operation mode A; and cell voltage in operation mode B with different CO_2-loaded solutions at different load ratios (PDF)

■ AUTHOR INFORMATION

Corresponding Author

Philipp Kuntke − *Wetsus, European Centre of Excellence for Sustainable Water Technology, 8900CC Leeuwarden, The Netherlands; Environmental Technology, Wageningen University, 6700 AA Wageningen, The Netherlands;* orcid.org/0000-0002-2342-8662; Email: philipp.kuntke@wur.nl

Authors

Mu Lin − *Wetsus, European Centre of Excellence for Sustainable Water Technology, 8900CC Leeuwarden, The Netherlands; Environmental Technology, Wageningen University, 6700 AA Wageningen, The Netherlands*

Clément Ehret − *Wetsus, European Centre of Excellence for Sustainable Water Technology, 8900CC Leeuwarden, The Netherlands*

Hubertus V. M. Hamelers − *Wetsus, European Centre of Excellence for Sustainable Water Technology, 8900CC Leeuwarden, The Netherlands; Environmental Technology, Wageningen University, 6700 AA Wageningen, The Netherlands;* orcid.org/0000-0002-0990-4773

Annemiek ter Heijne − *Wetsus, European Centre of Excellence for Sustainable Water Technology, 8900CC Leeuwarden, The Netherlands; Environmental Technology, Wageningen University, 6700 AA Wageningen, The Netherlands;* orcid.org/0000-0002-6882-8395

Complete contact information is available at: https://pubs.acs.org/10.1021/acssuschemeng.3c08430

Notes

The authors declare no competing financial interest.

■ ACKNOWLEDGMENTS

This work was performed in the cooperation framework of Wetsus, European Centre of Excellence for Sustainable Water Technology (www.wetsus.eu). Wetsus is cofunded by the Dutch Ministry of Economic Affairs and Ministry of Infrastructure and Environment, the European Union Regional Development Fund, the Province of Fryslân, and the Northern Netherlands Provinces. The authors would like to thank the participants of the research theme "Sustainable Carbon Cycle" for fruitful discussions and financial support and Ir. John Ferwerda for the technical support. This work was also supported by ConsenCUS project ("Carbon Neutral clusters by Electricity-based innovation in Capture, Utilization and Storage" www.consencus.eu). The ConsenCUS project has received funding from the European Union's Horizon 2020 Research and Innovation program under Grant Agreement no. 101022484.

■ REFERENCES

(1) Liu, Y.; Ye, H.-Z.; Diederichsen, K. M.; Van Voorhis, T.; Hatton, T. A. Electrochemically mediated carbon dioxide separation with quinone chemistry in salt-concentrated aqueous media. *Nat. Commun.* **2020**, *11*, 2278.

(2) Voskian, S.; Hatton, T. A. Faradaic electro-swing reactive adsorption for CO 2 capture †. *Energy Environ. Sci.* **2019**, *12*, 3530−3547.

(3) Ozkan, M.; Nayak, S. P.; Ruiz, A. D.; Jiang, W. Current status and pillars of direct air capture technologies. *iScience* **2022**, *25*, 103990.

(4) Hashimoto, K. *Global Temperature and Atmospheric Carbon Dioxide Concentration*; Springer, 2019; pp 5−17.

(5) Arias, P.; Bellouin, N.; Coppola, E.; Jones, R.; Krinner, G.; Marotzke, J.; Naik, V.; Palmer, M.; Plattner, G.-K.; Rogelj, J.; Rojas, M.; Sillmann, J.; Storelvmo, T.; Thorne, P.; Trewin, B.; Rao, K.; Adhikary, B.; Allan, R.; Armour, K.; Zickfeld, K. *IPCC AR6 WGI Technical Summary*, 2021; pp 33−144.

(6) Le Quéré, C.; Jackson, R. B.; Jones, M. W.; Smith, A. J. P.; Abernethy, S.; Andrew, R. M.; De-Gol, A. J.; Willis, D. R.; Shan, Y.; Canadell, J. G.; Friedlingstein, P.; Creutzig, F.; Peters, G. P. Temporary reduction in daily global CO2 emissions during the

COVID-19 forced confinement. *Nat. Clim. Change* **2020**, *10*, 647−653.
(7) Jiang, K.; Ashworth, P.; Zhang, S.; Hu, G. Print media representations of carbon capture utilization and storage (CCUS) technology in China. *Renew. Sustain. Energy Rev.* **2022**, *155*, 111938.
(8) Breyer, C.; Fasihi, M.; Bajamundi, C.; Creutzig, F. Direct Air Capture of CO2: A Key Technology for Ambitious Climate Change Mitigation. *Joule* **2019**, *3*, 2053−2057.
(9) Wang, M.; Hariharan, S.; Shaw, R. A.; Hatton, T. A. Energetics of electrochemically mediated amine regeneration process for flue gas CO2 capture. *Int. J. Greenh. Gas Control* **2019**, *82*, 48−58.
(10) Meng, F.; Meng, Y.; Ju, T.; Han, S.; Lin, L.; Jiang, J. Research progress of aqueous amine solution for CO2 capture: A review. *Renew. Sustain. Energy Rev.* **2022**, *168*, 112902.
(11) House, K. Z.; Harvey, C. F.; Aziz, M. J.; Schrag, D. P. The energy penalty of post-combustion CO2 capture & storage and its implications for retrofitting the U.S. installed base. *Energy Environ. Sci.* **2009**, *2*, 193−205.
(12) Vevelstad, S. J.; Buvik, V.; Knuutila, H. K.; Grimstvedt, A.; Da Silva, E. F. Important Aspects Regarding the Chemical Stability of Aqueous Amine Solvents for CO2Capture. *Ind. Eng. Chem. Res.* **2022**, *61*, 15737−15753.
(13) Rahimi, M.; Khurram, A.; Hatton, T. A.; Gallant, B. Electrochemical carbon capture processes for mitigation of CO 2 emissions. *Chem. Soc. Rev.* **2022**, *51*, 8676−8695.
(14) Hatton, T. (Invited) Electrochemically Modulated Mitigation of Acid Gas Emissions. *ECS Meeting Abstracts MA2021-02*, 2021; p 749.
(15) Intergovernmental Panel on Climate Change. *Climate Change 2014 Synthesis Report: Summary for Policy Makers*, 2014.
(16) Apaydin, D. H.; Głowacki, E. D.; Portenkirchner, E.; Sariciftci, N. S. Direct Electrochemical Capture and Release of Carbon Dioxide Using an Industrial Organic Pigment: Quinacridone. *Angew. Chem., Int. Ed.* **2014**, *53*, 6819−6822.
(17) Ranjan, R.; Olson, J.; Singh, P.; Lorance, E. D.; Buttry, D. A.; Gould, I. R. Reversible Electrochemical Trapping of Carbon Dioxide Using 4,4′-Bipyridine That Does Not Require Thermal Activation. *J. Phys. Chem. Lett.* **2015**, *6*, 4943−4946.
(18) Rahimi, M.; Diederichsen, K. M.; Ozbek, N.; Wang, M.; Choi, W.; Hatton, T. A. An Electrochemically Mediated Amine Regeneration Process with a Mixed Absorbent for Postcombustion CO2Capture. *Environ. Sci. Technol.* **2020**, *54*, 8999−9007.
(19) Kuntke, P.; Rodríguez Arredondo, M.; Widyakristi, L.; Ter Heijne, A.; Sleutels, T. H. J. A.; Hamelers, H. V. M.; Buisman, C. J. N. Hydrogen Gas Recycling for Energy Efficient Ammonia Recovery in Electrochemical Systems. *Environ. Sci. Technol.* **2017**, *51*, 3110−3116.
(20) Shu, Q.; Legrand, L.; Kuntke, P.; Tedesco, M.; Hamelers, H. V. M. Electrochemical Regeneration of Spent Alkaline Absorbent from Direct Air Capture. *Environ. Sci. Technol.* **2020**, *54*, 8990−8998.
(21) Jeremiasse, A. W.; Hamelers, H. V. M.; Kleijn, J. M.; Buisman, C. J. N. Use of Biocompatible Buffers to Reduce the Concentration Overpotential for Hydrogen Evolution. *Environ. Sci. Technol.* **2009**, *43*, 6882−6887.
(22) Muroyama, A. P.; Gubler, L. Carbonate Regeneration Using a Membrane Electrochemical Cell for Efficient CO2 Capture. *ACS Sustain. Chem. Eng.* **2022**, *10*, 16113−16117.
(23) Muroyama, A. P.; Beard, A.; Pribyl-Kranewitter, B.; Gubler, L. Separation of CO2 from Dilute Gas Streams Using a Membrane Electrochemical Cell. *ACS ES&T Eng.* **2021**, *1*, 905−916.
(24) Auinger, M.; Katsounaros, I.; Meier, J. C.; Klemm, S. O.; Biedermann, P. U.; Topalov, A. A.; Rohwerder, M.; Mayrhofer, K. J. J. Near-surface ion distribution and buffer effects during electrochemical reactions. *Phys. Chem. Chem. Phys.* **2011**, *13*, 16384−16394.
(25) Yin, F.; Fang, L.; Liu, H. pH Overpotential for Unveiling the pH Gradient Effect of H+/OH- Transport in Electrode Reaction Kinetics. *CCS Chem.* **2022**, *4*, 369−380.
(26) Strmcnik, D.; Uchimura, M.; Wang, C.; Subbaraman, R.; Danilovic, N.; Van Der Vliet, D.; Paulikas, A. P.; Stamenkovic, V. R.; Markovic, N. M. Improving the hydrogen oxidation reaction rate by promotion of hydroxyl adsorption. *Nat. Chem.* **2013**, *5*, 300−306.
(27) Sheng, W.; Zhuang, Z.; Gao, M.; Zheng, J.; Chen, J. G.; Yan, Y. Correlating hydrogen oxidation and evolution activity on platinum at different pH with measured hydrogen binding energy. *Nat. Commun.* **2015**, *6*, 5848.
(28) Jeremiasse, A. W.; Hamelers, H. V. M.; Kleijn, J. M.; Buisman, C. J. N. Use of biocompatible buffers to reduce the concentration overpotential for hydrogen evolution. *Environ. Sci. Technol.* **2009**, *43*, 6882−6887.
(29) Sheng, W.; Zhuang, Z.; Gao, M.; Zheng, J.; Chen, J. G.; Yan, Y. Correlating hydrogen oxidation and evolution activity on platinum at different pH with measured hydrogen binding energy. *Nat. Commun.* **2015**, *6*, 5848.
(30) Santarelli, M. G.; Torchio, M. F.; Cochis, P. Parameters estimation of a PEM fuel cell polarization curve and analysis of their behavior with temperature. *J. Power Sources* **2006**, *159*, 824−835.
(31) Durst, J.; Simon, C.; Hasché, F.; Gasteiger, H. A. Hydrogen Oxidation and Evolution Reaction Kinetics on Carbon Supported Pt, Ir, Rh, and Pd Electrocatalysts in Acidic Media. *J. Electrochem. Soc.* **2015**, *162*, F190−F203.
(32) Strathmann, H. Preparation and Characterization of Ion-Exchange Membranes. In *Membrane Science and Technology*; Elsevier, 2004, Chapter 3; pp 89−146.
(33) Stec, M.; Tatarczuk, A.; Więcław-Solny, L.; Krótki, A.; Spietz, T.; Wilk, A.; Śpiewak, D. Demonstration of a post-combustion carbon capture pilot plant using amine-based solvents at the Łaziska Power Plant in Poland. *Clean Technol. Environ. Policy* **2016**, *18*, 151−160.
(34) Vega, F.; Cano, M.; Gallego, L. M.; Camino, S.; Camino, J. A.; Navarrete, B. Evaluation of MEA 5 M performance at different CO2 concentrations of flue gas tested at a CO2 capture lab-scale plant. *Energy Procedia* **2017**, *114*, 6222−6228.
(35) Sanchez Fernandez, E.; Heffernan, K.; Van Der Ham, L. V.; Linders, M. J. G.; Eggink, E.; Schrama, F. N. H.; Brilman, D. W. F.; Goetheer, E. L. V.; Vlugt, T. J. H. Conceptual design of a novel CO2 capture process based on precipitating amino acid solvents. *Ind. Eng. Chem. Res.* **2013**, *52*, 12223−12235.
(36) Gladis, A.; Lomholdt, N. F.; Fosbøl, P. L.; Woodley, J. M.; von Solms, N. Pilot scale absorption experiments with carbonic anhydrase-enhanced MDEA- Benchmarking with 30 wt% MEA. *Int. J. Greenh. Gas Control* **2019**, *82*, 69−85.
(37) Marcandalli, G.; Boterman, K.; Koper, M. T. M. Understanding hydrogen evolution reaction in bicarbonate buffer. *J. Catal.* **2022**, *405*, 346−354.
(38) Muroyama, A. P.; Abu-Arja, D.; Rogerio, B. K.; Masiello, D.; Winzely, M.; Gubler, L. Performance Enhancement of a Membrane Electrochemical Cell for CO_2 Capture. *J. Electrochem. Soc.* **2024**, *171*, 013504.
(39) Swiegers, G. F.; Terrett, R. N. L.; Tsekouras, G.; Tsuzuki, T.; Pace, R. J.; Stranger, R. The prospects of developing a highly energy-efficient water electrolyser by eliminating or mitigating bubble effects. *Sustain. Energy Fuels* **2021**, *5*, 1280−1310.
(40) Cooper, K. R.; Smith, M. Electrical test methods for on-line fuel cell ohmic resistance measurement. *J. Power Sources* **2006**, *160*, 1088−1095.
(41) Reshetenko, T.; Odgaard, M.; Schlueter, D.; Serov, A. Analysis of alkaline exchange membrane fuel cells performance at different operating conditions using DC and AC methods. *J. Power Sources* **2018**, *375*, 185−190.
(42) Santarelli, M. G.; Torchio, M. F.; Cochis, P. Parameters estimation of a PEM fuel cell polarization curve and analysis of their behavior with temperature. *J. Power Sources* **2006**, *159*, 824−835.

https://doi.org/10.1021/acssuschemeng.3c08430
ACS Sustainable Chem. Eng. 2024, 12, 7309−7317